ADVANCED OPTICAL MATERIALS
www.advopticalmat.de

Intramolecular Through-Space Charge-Transfer Effect for Achieving Room-Temperature Phosphorescence in Amorphous Film

Dehai Dou, Xin Zhou, Tian Wang, Qiqi Yang, Xiao Tan, Zhitian Ling, Marvin Manz, Xiaomin Liu, Gert-Jan A. H. Wetzelaer, Xiaosong Li, Martin Baumgarten, Paul W. M. Blom,* and Yungui Li**

Organic emitters that exhibit room-temperature phosphorescence (RTP) in neat films have application potential for optoelectronic devices, bio-imaging, and sensing. Due to molecular vibrations or rotations, the majority of triplet excitons recombine rapidly via non-radiative processes in purely organic emitters, making it challenging to observe RTP in amorphous films. Here, a chemical strategy to enhance RTP in amorphous neat films is reported, by utilizing through-space charge-transfer (TSCT) effect induced by intramolecular steric hindrance. The donor and acceptor groups interact via spatial orbital overlaps, while molecular motions are suppressed simultaneously. As a result, triplets generated under photo-excitation are stabilized in amorphous films, contributing to phosphorescence even at room temperature. The solvatochromic effect on the steady-state and transient photoluminescence reveals the charge-transfer feature of involved excited states, while the TSCT effect is further experimentally resolved by femtosecond transient absorption spectroscopy. The designed luminescent materials with pronounced TSCT effect show RTP in amorphous films, with lifetimes up to ≈40 ms, comparable to that in a rigid polymer host. Photoluminescence afterglow longer than 3 s is observed in neat films at room temperature. Therefore, it is demonstrated that utilizing intramolecular steric hindrance to stabilize long-lived triplets leads to phosphorescence in amorphous films at room temperature.

1. Introduction

Phosphorescence in organic luminescent materials intrinsically stems from the radiative transitions of triplet excitons to the ground state. However, because of Pauli's exclusion principle, this radiative process is spin-forbidden, generally slow, and can be easily outcompeted by faster non-radiative molecular relaxations at room temperature.[1] Organometallic phosphorescence emitters incorporating iridium, platinum, or gold have been intensively investigated and successfully applied as triplet harvesters for highly efficient organic light-emitting diodes. Because of the heavy atom effect, the spin-orbit coupling is significantly enhanced to achieve intersystem crossing (ISC) transition from singlet to triplet states, followed by radiative triplet decay, resulting in highly efficient room-temperature phosphorescence (RTP).[2–6] However, heavy atoms involved in these materials raise concerns about environmental sustainability as well as material costs.

For purely organic RTP emitters, the probability of triplet radiative transition is low leading to inferior phosphorescence quantum yields.[7,8] Ultralong afterglow from purely organic RTP emitters lasting up to several seconds has been reported, contrasting with spin-allowed radiative singlet transitions in the nanosecond region, referred to as prompt fluorescence (PF).[9–12] It is worth noting that purely organic luminescent materials without heavy atoms can only show RTP emission whenever molecular vibrations and non-radiative transitions are effectively suppressed, such as in crystals or a rigid polymer matrix.[10,13–17] However, it is difficult to use crystals in optoelectronic devices, since doping in rigid polymers can potentially bring disadvantages such as phase separation or inhomogeneity.[18] Long-lived RTP in amorphous films can avoid the aforementioned problems and is therefore highly desirable. On the other hand, it is a scientific challenge to stabilize long-lived triplets in amorphous films, because of the more pronounced molecular non-radiative motions as compared to that in a rigid host, while suppressing non-radiative decay from

D. Dou, X. Zhou, Q. Yang, X. Tan, Z. Ling, M. Manz, X. Liu, G.-J. A. H. Wetzelaer, M. Baumgarten, P. W. M. Blom, Y. Li
Max Planck Institute for Polymer Research
Ackermannweg 10, 55128 Mainz, Germany
E-mail: martin.baumgarten@mpip-mainz.mpg.de; blom@mpip-mainz.mpg.de; yungui.li@mpipmainz.mpg.de
T. Wang, X. Li
Department of Chemistry
University of Washington
Seattle, WA 98195-1700, USA

The ORCID identification number(s) for the author(s) of this article can be found under https://doi.org/10.1002/adom.202400976

DOI: 10.1002/adom.202400976

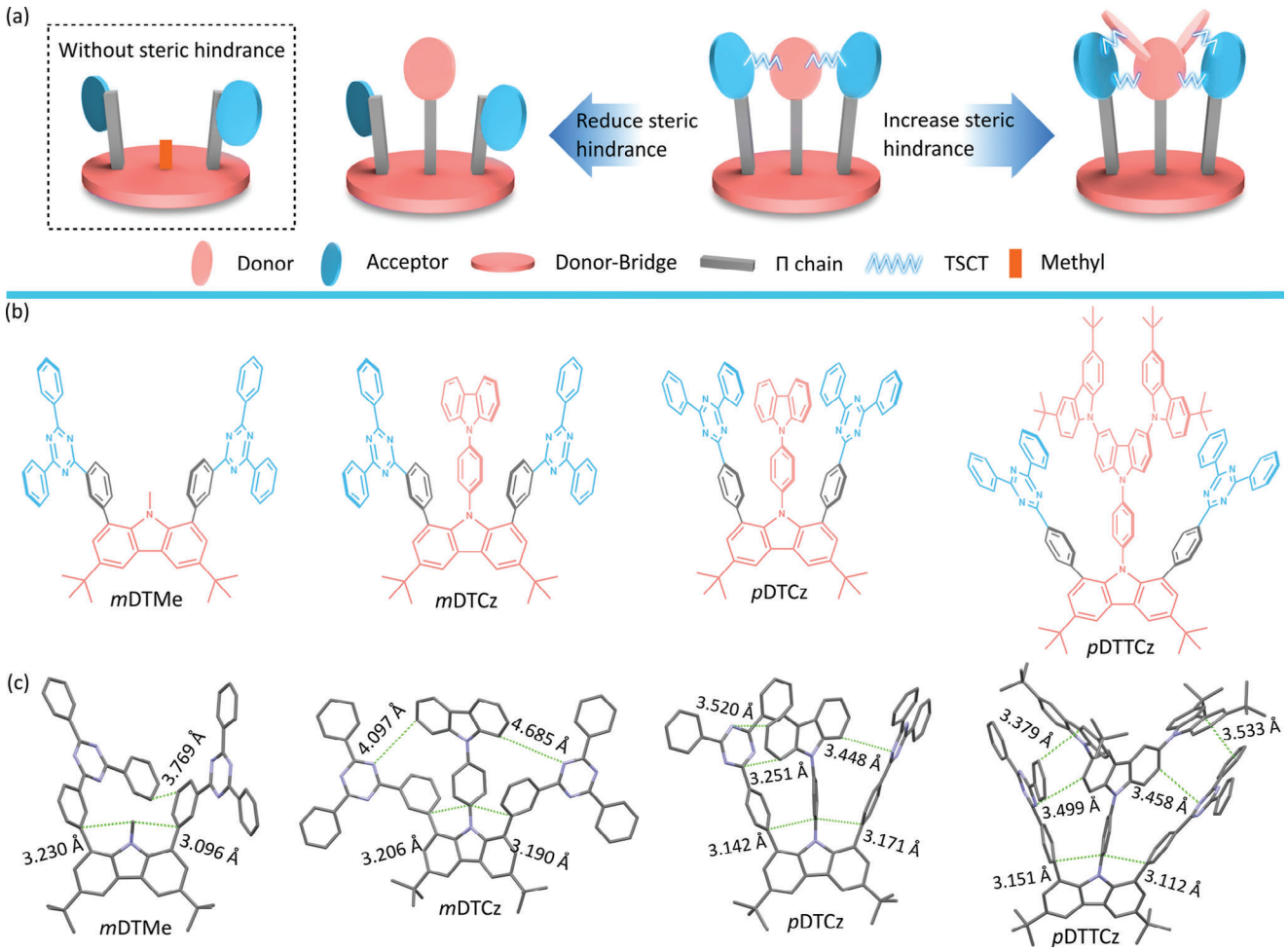

Figure 1. Chemical design principle. a) Schematic illustration of steric hindrance-induced TSCT. b) Chemical structure of *m*DTMe, *m*DTCz, *p*DTCz, and *p*DTTCz. c) Geometrical configuration of *m*DTMe, *m*DTCz, *p*DTCz, and *p*DTTCz in single crystals with intramolecular interactions.

triplets is of vital significance for optoelectronic devices including organic light-emitting diodes or organic solar cells.[7,19,20] Therefore, the development of phosphorescent materials in neat films with long-lived triplets remains a formidable challenge from the application or scientific perspective.[21] In recent years, scientific effects have been dedicated to realize RTP in amorphous films.[22–25]

Charge-transfer (CT) states in donor–acceptor-based organic emitters have been intensively investigated for the development of thermally activated delayed fluorescence (TADF) materials.[26,27] When the conjugation between the donor and acceptor group is disturbed either by tuning the link position or geometric configurations with pronounced steric hindrance, singlet and triplet excitons can show a mixture of CT and locally excited (LE) features.[28] However, it is noted that for many donor-acceptor type emitters, the notorious aggregation-induced quenching can lead to pronounced PLQY reduction.[28] In some extreme cases, either TADF or RTP emission is reduced to the detection limit or even fully quenched, because of the overwhelming non-radiative triplet decay.[29] Efficient TADF emission originating from the through-space CT (TSCT) state has been demonstrated when the donor and acceptor groups are linked to a non-conjugated backbone.[30,31] In such a molecular design, charge transfer happens from the donor to the acceptor group through space. A dense molecular packing is beneficial for the TSCT-induced emission in this case, stabilizing the long-lived triplet states which contribute to efficient TADF emission in polymeric neat films.[32]

In the present work, we demonstrate a general method to achieve purely organic luminescent materials with RTP emission in amorphous neat films by utilizing the TSCT effect, induced by intramolecular steric hindrance between the donor and acceptor moieties. The design principle is schematically presented in **Figure 1**a. The molecular linking bridge is a rigid linker (tert-butylcarbazole) connecting donor and acceptor units. By tuning the relative position between a rigid linker and acceptor groups, or by adjusting the size of the donor moiety, the steric hindrance effect and photophysical properties are modified. As a result, RTP emission in purely organic molecules with a lifetime of up to 40 ms has been realized in thermally evaporated neat films, which is comparable to that when buried in a rigid polymer host. We further show that the tuned RTP decay in neat films can be applied for time-dependent luminescent patterns, which can be used for data-safety applications in the future.

2. Results and Discussion

2.1. Synthesis and Structural Characterization

In the present study, the donor consists of carbazole/tricarbazole groups, while the acceptor part is based on the triazine core since they exhibit promising long-lived triplets, which have been used previously for building TADF and RTP materials.[10,11,33,34] The chemical structure of developed materials in the present study is shown in Figure 1b, with short names as *m*DTMe, *m*DTCz, *p*DTCz, and *p*DTTCz, respectively. The full name can be found in the Supplementary Information. These materials are synthesized with well-known reactions with high product yields, including Ullmann reaction to build donor groups with carbazole/methyl, and Suzuki coupling to link the donor and acceptor groups to obtain the target compounds shown in Figure 1b. Their chemical structures are characterized and confirmed by ^{1}H and ^{13}C NMR spectroscopy (Figure S1–S18, Supporting Information), high-resolution mass spectrometry (HRMS) (Figure S19, Supporting Information), and single-crystal X-ray diffractions (Figure 1c; Tables S1 and S2, Supporting Information). High purity has been confirmed by high-performance liquid chromatography, as shown in Figure S20 (Supporting Information).

Intramolecular weak interactions for developed materials in single crystals are presented in Figure 1c, while their space-filling structures indicating the intramolecular geometric confinement are shown in Figure S19 (Supporting Information). Pronounced steric hindrance effects have been observed in the *p*DTCz and *p*DTTCz single-crystal structures. The carbazole and triazine unit are aligned in an edge-to-edge configuration for *p*DTCz, with close confocal π-π stacking of two fragments in a distance ≈3.251–3.520 Å (Figure 1c). Because of the geometric confinement and close spatial distance, the intramolecular π-π interactions between the carbazole/tricarbazole donor and the triazine acceptor can be visualized in *p*DTCz and *p*DTTCz, as indicated in Figure 1c and Figure S21 (Supporting Information). Such a close spatial distance indicates the presence of TSCT interactions between the carbazole donor and triazine acceptors.

In contrast, in *m*DTCz, because the tert-butyl carbazole moiety is linked to the meta-position of the benzene ring linking the triazine moiety, there is no proper edge-to-edge alignment between the carbazole and triazine groups. As summarized in Tables S1 and S2 (Supporting Information), the crystal density is 1.152 g m^{-3} for *m*DTMe without TSCT effect, while the density is even lower for 0.970 g m^{-3} for *p*DTTCz with the strongest TSCT effect. Distances from the top carbazole unit to the nearby triazine rings are 4.097 and 4.685 Å, respectively, large enough for possible molecular rotations or vibrations to some extent (Figure 1c). Because of the slightly longer distance between the carbazole and triazine unit, the intramolecular interaction is weaker compared to that in *p*DTCz and *p*DTTCz (Figure S21, Supporting Information). However, for *m*DTMe, since there is no additional carbazole group, the triazine moiety can rotate or vibrate more easily (Figure 1c).

For *p*DTCz crystals, two individual molecules show a head-to-tail staggered arrangement with the closest distance of 3.475 Å from the carbazolyl-bridge to the trazine acceptor of the closest molecule, which might induce weak intermolecular interactions (Figure S21, Supporting Information). Nevertheless, intermolecular interactions are not unexpected in general, since molecular movements are significantly suppressed in crystals.[35,36] After ultraviolet (UV) irradiation, the photoluminescence intensity only decreases gradually with a long lifetime, still observable up to 42 s, indicating ultralong afterglow emission in crystals at room temperature, as shown in Figure S22 (Supporting Information). The detailed data about the molecular packing for these developed materials in single crystals are summarized in Tables S1 and S2 (Supporting Information).

2.2. Basic Properties

The steady-state ultraviolet-visible (UV-vis) absorption and photoluminescence (PL) are shown in **Figures 2**a–c and S23 (Supporting Information). In toluene, the four molecules *m*DTMe, *m*DTCz, *p*DTCz, and *p*DTTCz exhibit broad absorption in the 330–400 nm range attributed to π-π^* and CT from the carbazole/tert-butylcarbazole bridge/tricarbazole to the triazine acceptor transitions.[26] When dissolved in different solvents, the steady-state PL spectra are red-shifted when the solvent polarity increases. Shoulder peak at ≈400 nm has been observed in n-hexane, which has also been observed in emitters with donor and acceptor units.[37] Moreover, there is a gradual increase of the decay lifetime of PF when the solvent polarity rises, as shown in Figure S24 (Supporting Information). The fitted PF lifetime for these materials in different solvents is summarized in Table S4 (Supporting Information). The polarity-dependent fluorescence properties indicate the CT feature of singlet states.[34,38] The solvatochromism mainly results from the difference of dielectric properties in surrounding solvent molecules, which in the end affects the excited states of organic emitters in terms of the electron cloud distribution and therefore the optical properties.[37] Besides, the developed materials show excellent thermal stability, with the decomposition temperature (5% weight loss) T_d of 474 °C for *m*DTCz, 493 °C for *p*DTCz, and 533 °C for *p*DTTCz, respectively (Figure S27, Supporting Information).

The absolute PL quantum yields (PLQY) for thermally deposited neat films are determined using an integrating sphere under nitrogen and ambient atmosphere. In nitrogen, the PLQY is 36.9% for the *m*DTMe neat film, while it increases to 48.0% for *m*DTCz, 54.9% for *p*DTCz, and further to 73.5% for *p*DTTCz (**Table 1**; Table S3, Supporting Information). The gradual increase of PLQY is consistent with the change of intramolecular interactions in crystals, as schematically illustrated in Figure 1c, which suppresses the non-radiative molecular relaxations.[28] The PLQY is reduced slightly with 3–6% when measured in ambient atmosphere as compared to that in nitrogen, indicating the involvement of triplets. As summarized in Table S5 (Supporting Information), the PLQY in nitrogen for emitters when being buried in a polymer host increases from 45.7% for *m*DTMe to 88.3% for *p*DTTCz. Therefore, in the PMMA matrix, PLQY increases for materials with more pronounced steric hindrance, similar to that observed in amorphous films.

The delayed PL spectra after the excitation pulse of 200 µs, treated as the RTP spectra, are plotted in Figure S23 (Supporting Information) for *m*DTMe (in PMMA) and in Figure 2d for

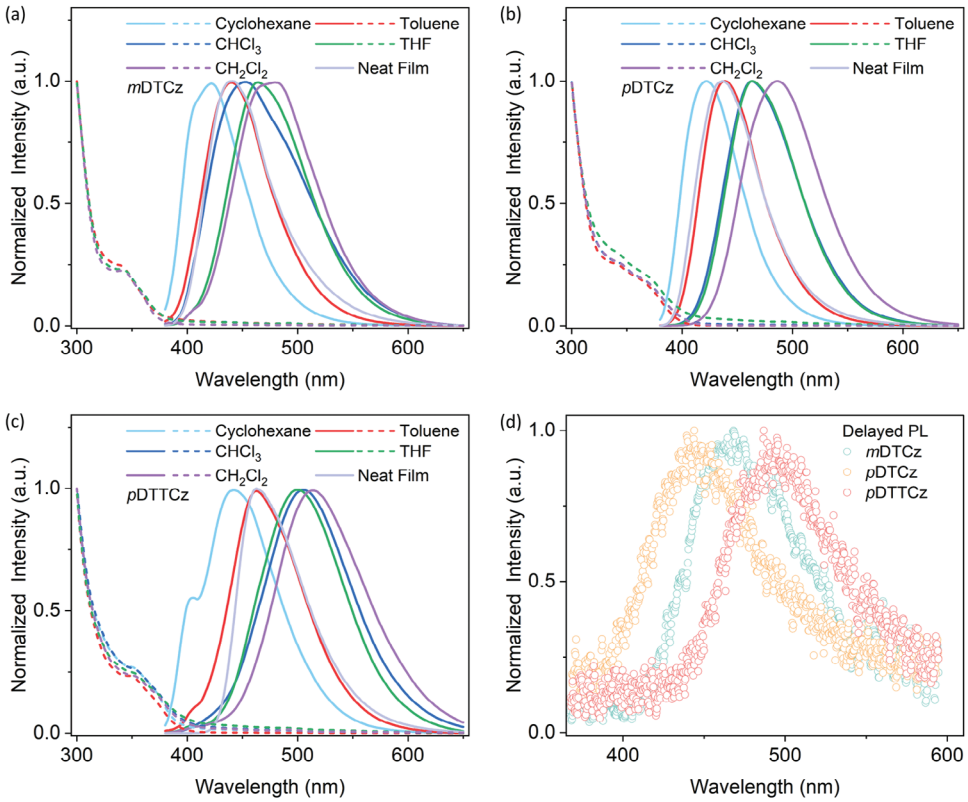

Figure 2. Basic photophysical properties. Steady-state absorption (dashed) and PL spectra (solid) for a) *m*DTCz, b) *p*DTCz, and c) *p*DTTCz. (d) The phosphorescence spectra with a delay of 200 µs after the excitation, were measured in N_2 with thermally evaporated films at room temperature.

*m*DTCz, *p*DTCz, and *p*DTTCz neat films, respectively. These phosphorescence spectra, with peaks at ≈440 to 500 nm, are relatively different from previous reports of phosphorescence from the carbazole or triazine groups, but quite close to the reported delayed emission from compounds with the carbazole/tert-butylcarbazole donor and triazine acceptor.[10,39] The singlet and triplet energy are determined according to the lineshape analysis from the fluorescence and phosphorescence spectra, as shown in Figure S25 (Supporting Information) and Table 1. The singlet-triplet splitting energy ΔE_{ST} of *m*DTCz, *p*DTCz, and *p*DTTCz is 0.10, 0.11, and 0.04 eV, respectively. The basic photophysical properties of these four emitters are summarized in Table 1 and Table S3 (Supporting Information).

2.3. Theoretical Calculations

To better understand the photophysical properties of these molecules, we investigate the excited-state properties by employing time-dependent density functional theory (TD-DFT) on *m*DTMe, *m*DTCz, *pD* TCz, and *p*DTTCz. The frontier molecular orbitals (FMOs) and the first excited-state electron distributions at the ground-state geometry are shown in Figure S28 (Supporting Information). The highest occupied molecular orbital (HOMO) of each molecule in the ground-state geometry is mainly located at the donor unit, while for *p*DTTCz there is almost no distribution on the tert-butyl carbazole bridge. The lowest unoccupied molecular orbital (LUMO) is predominantly distributed on the acceptor section (Figure S28, Supporting Information). The excitation energies of the first excited state at the ground-state geometry match with the experimental absorption peaks, as shown in Table 1 and Table S6 (Supporting Information). Furthermore, the singlet and triplet energy levels are modeled by examining the excitation energies at first excited-state-minimum geometries. Based on the excited-state-minimum geometries the calculated S_1 and T_1 energy levels (Table S6, Supporting Information), the ΔE_{ST} between the S_1 and T_1 for *m*DTMe, *m*DTCz, *p*DTCz, and *p*DTTCz is estimated as

Table 1. Photophysical properties of *m*DTCz, *p*DTCz, and *p*DTTCz.

Sample	λ_{Abs} [nm][a]	λ_{FL} [nm][b]	λ_{FL} [nm][a]	λ_{FL} [nm][c]	λ_{FL} [nm][d]	λ_{FL} [nm][e]	λ_{FL} [nm][f]	λ_{PH} [nm][g]	PLQY Air / N_2 [%][f]	S_1 / T_1 [eV]
*m*DTCz	341/357	421	438	453	464	483	441	470	43.8 / 48.0	2.90 / 2.80
*p*DTCz	340/367	422	438	463	463	487	437	443	50.3 / 54.9	2.92 / 2.81
*p*DTTCz	352/371	441	462	504	499	514	463	481	67.2 / 73.5	2.84 / 2.80

[a] in toluene; [b] in cyclohexane; [c] in $CHCl_3$; [d] in THF; [e] in CH_2Cl_2; [f] Neat film; [g] Phosphorescence (PH) peak of neat film at room temperature.

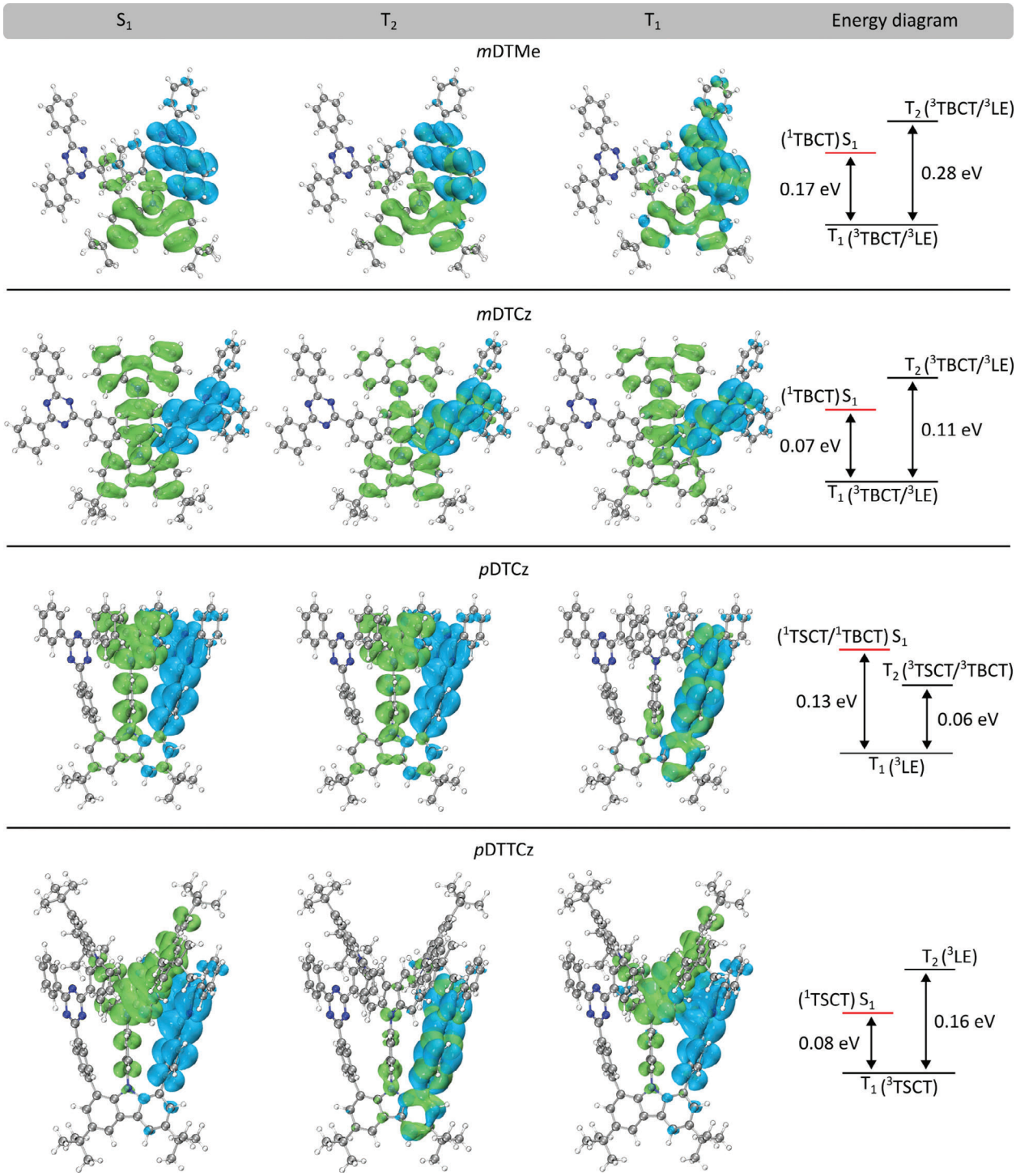

Figure 3. Hole (green) and electron (blue) spatial distribution and calculated energy levels for *m*DTMe, *m*DTCz, *p*DTCz, and *p*DTTCz.

0.17, 0.07, 0.13, and 0.08 eV, respectively. It is noted that the additional higher-lying triplet state T_2 also has a very small energy difference with the singlet states.

To further understand the excited-state properties for *m*DTMe, *m*DTCz, *p*DTCz, and *p*DTTCz, we analyze the hole and electron distribution of S_1, T_2, and T_1, as shown in **Figure 3**. For *m*DTMe, the S_1 state primarily shows through-bond charge transfer (TBCT) nature, while triplet states T_2 and T_1 are composed of a mixture of locally excited (LE) and TBCT properties. For *m*DTCz, the electronic interaction between the carbazole and triazine units is weak due to the distance. The S_1 state shows mainly the TBCT nature, while triplet states T_2 and T_1 exhibit the

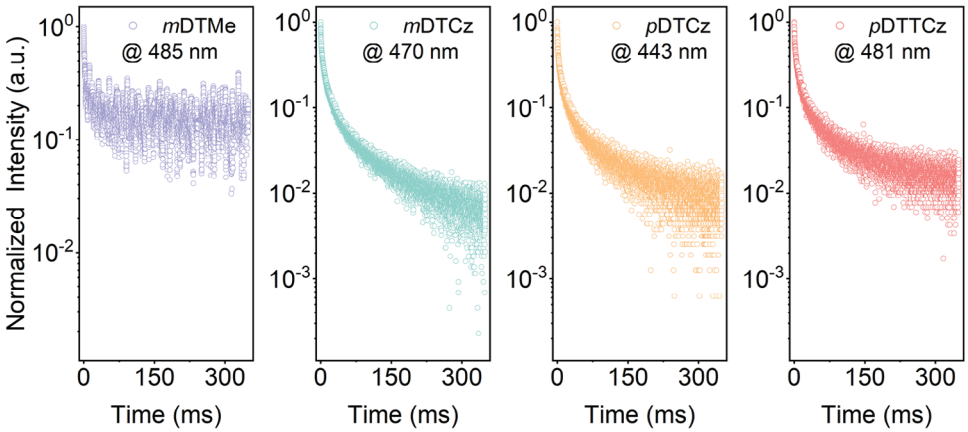

Figure 4. The RTP decay of amorphous films in the millisecond time window in N_2.

mixing properties of LE and TBCT, similar to *m*DTMe. The electronic wave functions of T_1 are mainly located at the phenyltriazine acceptor, but the hole wave function is mainly distributed in the carbazole groups. In *p*DTCz and *p*DTTCz the S_1 states show the characteristics of TSCT (carbazole/tricarbazole to triazine) with only minor involvement of tert-butyl carbazole bridges. Furthermore, it is noted that a pronounced TSCT character for *p*DTTCz T_1 is resolved, which might be induced by the proximity and steric hindrance. The LE and CT ratios of the S_1 and T_1 states are estimated by using the inter-fragment charge transfer (IFCT) method implemented in Multiwfn. We divide each individual molecule into two fragments: fragment 1 is the donor and fragment 2 is the two triazines. The IFCT method counts the electron and hole contribution from both fragment 1 and fragment 2. The difference between the number of electrons and holes in fragment 1 corresponds to the number of charges transferred from fragment 1 to fragment 2, whose ratio is defined as the CT ratio. Meanwhile, the ratio of charges localized on the same fragment is treated as the LE ratio. As summarized in Table S7 (Supporting Information), it is noted that the ratio of CT is as high as 76.4% in the T_1 state of *p*DTTCz.

2.4. Transient Photoluminescence

The impact of intramolecular steric hindrances on the transient photophysical properties of the developed materials is further studied. First, the transient PL decays in the nitrogen atmosphere for neat films prepared by thermal evaporation are investigated. As shown in **Figures** 4 and S29 (Supporting Information), the transient PL decay in nitrogen measured by time-correlated single-photon counting (TCSPC) indicates that there is PF emission in the nanosecond (ns) range, delayed fluorescence (DF) in the microsecond (μs) range, and RTP in the millisecond (ms) range. The fitted decay lifetime of these different components is summarized in **Table** 2. For these materials, the PF lifetime is ≈7–10 ns, and the DF lifetime is ≈1 μs. The RTP decay is further fitted starting from 80 μs, as shown in Figures S30 and S31 (Supporting Information), with the RTP decay lifetime of 4.78, 34.3, 36.5, and 41.9 ms for *m*DTMe, *m*DTCz, *p*DTCz, and *p*DTTCz, respectively. When being buried in a PMMA host, the decay lifetime of RTP is increased to 28.5 ms for *m*DTMe, 36.3 ms for *m*DTCz, 37.4 ms for *p*DTCz, and 49.4 ms for *p*DTTCz. The transient PL properties are summarized in Figure S32 and Table S8 (Supporting Information). For *m*DTMe, it is noted that the RTP lifetime is significantly enhanced in PMMA with a factor of ≈6 as compared to that in neat film, demonstrating the pronounced molecular motions in *m*DTMe neat film, consistent with the molecular packing results. As for *m*DTCz, *p*DTCz, and *p*DTTCz, the RTP lifetime is only slightly increased in the PMMA host. Such a comparison indicates that the molecular steric hindrance in *m*DTCz, *p*DTCz, and *p*DTTCz neat film is only slightly less effective compared to that in a rigid polymer host. The slightly longer intramolecular group distance in *m*DTCz can already largely suppress the non-radiative molecular motions, though comparably less effective compared to that in *p*DTCz and *p*DTTCz.

It is worth noting that the neat films prepared by thermal evaporation are amorphous without significant crystallinity signals, as confirmed by the X-ray diffraction (XRD), shown in Figure S26 (Supporting Information). Because of pronounced molecular movements with activation energy comparable with or even lower than the thermal energy at room temperature, non-radiative molecular relaxations in the form of vibrations or rotations can quench the phosphorescence radiation without rigid environmental confinement. However, due to the intramolecular steric hindrance effect, molecular rotations are effectively suppressed, contributing to the pronounced RTP emission even in amorphous films for *m*DTCz, *p*DTCz, and *p*DTTCz. As shown in Figure 4, for *m*DTMe neat film, there is no significant RTP decay, which is consistent with the absence of intramolecular steric

Table 2. The PL decay lifetime summary for amorphous neat films in air or nitrogen.

Sample	τ_{PF} [ns] Air/N_2	τ_{DF} [μs] Air/N_2	τ_{RTP} [ms] Air/N_2
*m*DTMe	–/7.17	–/0.54	–/4.78
*m*DTCz	8.49/8.43	0.85/1.11	31.2/34.3
*p*DTCz	7.86/7.92	0.72/0.87	34.7/36.5
*p*DTTCz	9.75/9.82	0.81/0.83	37.5/41.9

hindrance or TSCT effect, as discussed in previous sections. The reason for the slightly longer RTP decay of *p*DTTCz compared to *m*DTCz and *p*DTCz might arise from stronger intramolecular geometric confinements, which is also consistent with the PLQY trend.

Furthermore, it is noted that RTP emission can even be detected under ambient conditions for *m*DTCz, *p*DTCz, and *p*DTTCz neat films. As shown in Figures S33 and S34 (Supporting Information), the RTP decay is still observable in air, with a slightly shorter decay lifetime compared with that in nitrogen. The RTP decay lifetime is 31.2, 34.7, and 37.5 ms for *m*DTCz, *p*DTCz, and *p*DTTCz films measured in ambient conditions, respectively, which is summarized in Table 2. There is a slight decrease of the PLQY of ≈4–6% for *p*DTCz and *p*DTTCz when being measured in ambient conditions. In such a case, since the emissive triplets are even stabilized in dense neat films with pronounced RTP, whenever measured in an ambient atmosphere, the triplet contribution toward the PL in N_2 should be higher than 4–6%. Nevertheless, the ISC rates (k_{ISC}) of these molecules can be still estimated by assuming either only the singlets or triplets contribute to the non-radiative losses, as summarized in Table S9 (Supporting Information).[38] Under each assumption, it is noted that k_{ISC} rates for these emitters are similar. Such an estimation illustrates that the geometry confinement has no big impact on the ISC process. The gradually elongated RTP emission and increased quantum yields from *m*DTCz, *p*DTCz to *p*DTTCz should therefore result from the reduced non-radiative loss because of intramolecular steric hindrance.

As shown in Figure S35 (Supporting Information), the temperature-dependent PL decay shows that the delayed part in the microsecond regime increases when the temperature decreases. The increase of delayed components violates the temperature-dependent behavior of materials with TADF. Since the DF is thermally activated in TADF emitters, the intensity of DF will decrease when cooled down. For RTP emission, the phosphorescence lifetime and intensity increase when the non-radiative relaxations are suppressed by cooling down.

2.5. Ultrafast Charge-Transfer State Relaxation

The charge-transfer states involved in the developed molecules are further experimentally verified and investigated by femtosecond transient absorption (fs-TA) spectroscopy. The 2D fs-TA spectra for *m*DTMe, *m*DTCz, *p*DTCz, and *p*DTTCz in $CHCl_3$ solution are shown in Figure S36 (Supporting Information), while that in cyclohexane is presented in Figure S39 (Supporting Information). When measured in both solvents, pronounced excited state absorption (ESA) has been observed for all emitters.

The long-lived ESA signal from ≈10 ps till the detection time window limit ≈8 ns can be assigned to singlet and triplet absorption. Furthermore, for all four molecules, fast decays are observed in $CHCl_3$ from the femtosecond to picosecond (ps) region, shown in **Figures** 5a–d and S36 (Supporting Information). Such a fast decay signal is also observed when measured with a lower excitation laser intensity, presented in Figures S37 and S38 (Supporting Information). Such a cross-check experimentally verifies the presence of ultrafast excited-state decay in the ps region, excluding possible experimental artifacts.

In $CHCl_3$, for *m*DTMe and *m*DTCz, fast decay signals have been only observed in the NIR range, while for *p*DTCz and *p*DTTCz, fast decay signals have been observed both in the visible and NIR wavelength region, as shown in Figure 5a–d. However, the fast decay component vanished in the non-polar solvent cyclohexane, as shown in Figure S39 (Supporting Information). It is known that the CT state is stabilized in the polar solvent, with a large molecular geometry difference between the ground state and singlet state.[40] Considering the experimental observations of PL red-shift and elongated decay lifetime of PF in polar solvents, together with the theoretical investigation, the fast decay component in fs-TA can be reasonably assigned to CT state relaxations.

In $CHCl_3$, the CT state relaxation for *m*DTMe and *m*DTCz has a lifetime of 5.7 ps at 1300 nm for *m*DTMe and 3.9 ps at 1550 nm for *m*DTCz, as shown in Figure S40 (Supporting Information). Furthermore, it is found that for *m*DTMe and *m*DTCz, the CT state in the NIR range has the shortest decay lifetime. The relaxation lifetime of the CT state is 10.5 and 8.3 ps for *p*DTCz at 550 and 1550 nm, respectively. For *p*DTTCz in $CHCl_3$, the fast decay at 550 nm has a lifetime of 10.3 ps, while it is 19.1 ps at 1550 nm. The lifetimes of short-lived CT relaxations observed by fs-TA states are summarized in Table S10 (Supporting Information). The faster CT state relaxation in *m*DTMe or *m*DTCz as compared to that in *p*DTCz and *p*DTTCz is consistent with the larger molecular rotation space observed from the single crystal results and shorter RTP lifetime, as discussed in previous sections. Considering the molecular structures of the organic materials shown in Figure 1c, it is likely that the signal in the NIR range observed for all the four molecules developed in this work can be assigned to the relaxation of TBCT states, while that observed within the visible wavelength range for *p*DTCz and *p*DTTCz can be assigned to the TSCT state.

2.6. Origin of RTP Emission in Amorphous Films

Based on the above experimental and theoretical results, we here make a summary discussion regarding the molecular origin of the RTP emission in organic amorphous films. From the PLQY and single crystal results, the gradual increase of the intramolecular steric hindrance from *m*DTMe and *m*DTCz to *p*DTCz and *p*DTTCz suppresses non-radiative losses. The comparable ISC rates estimated in these materials indicate that the triplet generation rates are similar for all these compounds. Therefore, one can deduce that the triplet non-radiative rates in *p*DTCz and *p*DTTCz amorphous films are significantly reduced, which in the end leads to much longer RTP decay as compared to *m*DTMe.

From the steady-state PL, transient PL decay and transient fs-TA results in different solvents, we infer that TBCT states are involved in the singlet relaxations, while TSCT fast decay signals are resolved for *p*DTCz and *p*DTTCz in $CHCl_3$. As for the triplet states, the theoretical investigations indicate that there might be a mixture of LE and TSCT properties for *p*DTCz and *p*DTTCz. When assuming that the triplet state T_1 would exhibit mainly a LE character, there should be only a minor shift of the RTP spectra during the chemical modification from *m*DTMe to *p*DTCz and *p*DTTCz, since the electron distribution in that case is mainly locally located at either the donor or the acceptor group.[38]

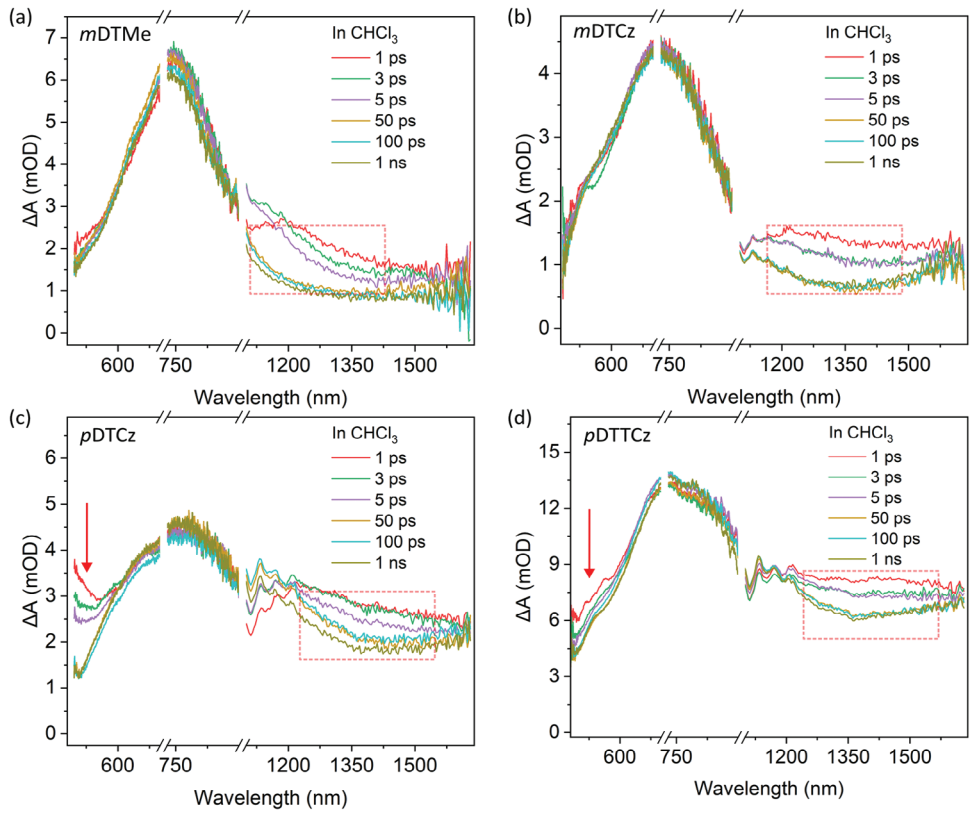

Figure 5. fs-TA spectroscopic characterization *m*DTMe, *m*DTCz, *p*DTCz, and *p*DTTCz. a), b), c), and d) selected TA spectra at specific delay times in $CHCl_3$. Measurements shown here are carried out with 100 µW fs-laser excitation at 360 nm. The arrow indicates the TSCT decay observed in *p*DTCz, and *p*DTTCz, while the dashed frames indicate the TBCT relaxation observed for all four emitters in $CHCl_3$.

However, as shown in Figure 2d, the phosphorescence spectra are quite different for *m*DTCz, *p*DTCz, and *p*DTTCz films, with similar molecular building blocks (donor and acceptor) but different molecular geometry structures. The reason is the different TSCT contributions to the T_1 states for these emitters due to the difference in intramolecular through-space interactions, which in the end leads to the phosphorescence spectral shift observed experimentally. Since the TSCT contribution is high in *p*DTTCz, as shown in Figures 2d and 3, its phosphorescence spectrum in neat film is largely shifted from the phosphorescent emission originating locally from the carbazole unit.[37]

It is noted that in the present study, the TSCT effect is induced within the single molecule, not the intermolecular packing in previous reports such as burying in crystals or polymer hosts. There are some previous reports about RTP emission from amorphous films.[18,41,42] It is further noted that the realization of RTP was either based on heavy atom effect, polymeric emitters, or by intermolecular weak bonding. Therefore, the intramolecular interactions in the present study are different from previous reports. Furthermore, the RTP decay lifetime is ≈40 ms in amorphous neat film prepared by thermally deposited. As a comparison, a recent work about RTP decay in amorphous films is ≈2.9 µs.[43] Therefore, the strategy developed in the present work by intramolecular TSCT effect is fundamentally different compared to previous reports by crystal engineering or polymeric host confinement. The RTP lifetime for materials with TSCT effect is comparable to that when being buried in a polymer host. In other words, the reduction of the intramolecular relaxation via TSCT effect can significantly elongate the triplet lifetime in an amorphous neat film, comparable to that reduced by a polymeric host.

2.7. Time-Dependent RTP Pattern from Neat Films

The fascinating PL properties of *m*DTMe, *m*DTCz, *p*DTCz, and *p*DTTCz in amorphous films might give new opportunities for different application scenarios. We here explore the possibility to fabricate time-dependent PL patterns based on these neat emissive materials. The synthesized materials are First dissolved and then drop-casted on pre-engraved substrates with different patterns. Though RTP emission has been detected under ambient conditions, time-dependent microscopy tests are carried out with materials encapsulated under a nitrogen atmosphere to observe afterglow with a longer lifetime. As shown in **Figure 6**, under UV light excitation, the filled alphabet pattern I, H, F, and E shows blue PL. After the stop of UV excitation, there is no phosphorescence emission from the pattern "I" with *m*DTMe, and clear delayed emission can still be resolved for patterns with *p*DTCz ("F") and *p*DTTCz ("E") after a delay of 3.08 s, whereas the pattern "H" with *m*DTCz is barely visible after such a long delay time. These results semi-quantitatively demonstrate that compounds

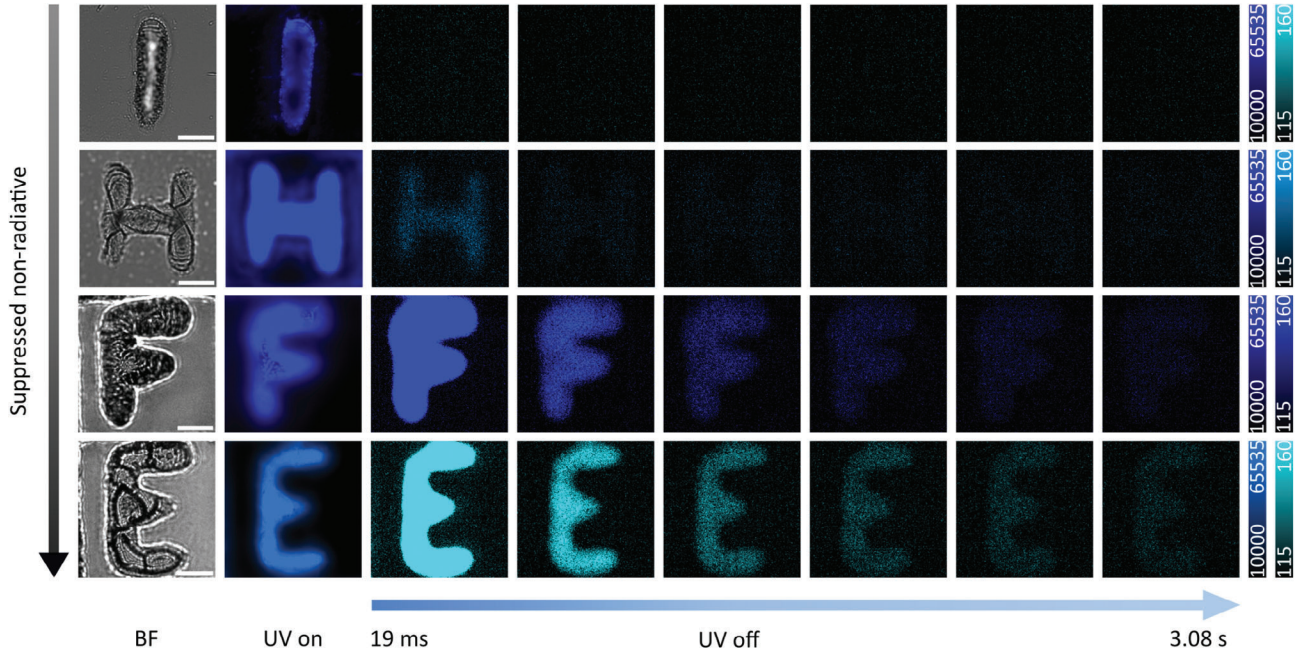

Figure 6. Time-resolved microscopy images based on neat materials after solvent evaporation. From top to bottom: *m*DTMe, *m*DTCz, *p*DTCz, and *p*DTTCz respectively. BF indicates a bright field without excitation. The scale bar is 10 µm. Color bar: left (UV on), right (UV off).

with stronger steric hindrance can elongate the RTP emission lifetime in pure films. Because of the afterglow lifetime difference, further combination with these materials in a single pattern can be used for building time-dependent luminescent patterns as a function of the delay time after UV excitation, which can be applied for data-safety applications in the future.

3. Conclusion

In conclusion, we demonstrated a molecular design strategy to stabilize long-lived emissive triplets in amorphous films by introducing an intramolecular steric hindrance effect. Four purely organic phosphorescent emitters were designed and synthesized based on carbazole donors and triazine acceptors, three of which showed pronounced phosphorescent decay from amorphous neat film at room temperature. Ultrafast relaxation of the through-space charge-transfer state has been observed by femtosecond transient absorption spectroscopy for emitters with pronounced intramolecular geometric confinement. Notably, efficient RTP emission with charge-transfer characteristics in amorphous films has been achieved, with an RTP decay lifetime of ≈40 ms, comparable to the lifetime achieved for these molecules embedded in the rigid polymer host PMMA. We believe that the molecular design strategy developed in the present study will facilitate the development of purely organic materials exhibiting RTP in amorphous films, with potential applications for data safety or optoelectronic devices.

4. Experimental Section

Synthesis: All chemicals and reagents were used as received from commercial resources (Sigma-Aldrich and BLD Pharmatech) without further purification. The target emitters were purified by sublimation and used for photophysic measurements.

Neat Film Deposition: Glass substrates (for PL and the transient PL decays), silicon substrates (for XRD), and quartz substrates (for PLQY) were treated with oxygen plasma for 20 min after being ultrasonically cleaned with acetone and isopropyl alcohol. Neat films were then thermally deposited in a vacuum chamber.

Steady State Absorption, PLQY, and Delayed PL Measurements: UV-vis absorption spectra were recorded on a Perkin-Elmer Lambda 900 spectrophotometer at room temperature. Steady-state PL spectra are measured on a HORIBA Jobin-Yvon Fluorolog 3–22 Tau-3, excited at 360 nm. PLQY was measured in a nitrogen-purged integrating sphere, based on a HORIBA Jobin-Yvon Fluorolog 3–22 Tau-3. Samples were excited at 360 nm and selected from an Xe-lamp. The measurement method was a standard method developed by de Mello et al.[44] The measurement was done based on three different configurations: a) the integrating sphere was empty; b) the sample was in place and the excitation beam was directed onto the sphere wall; c) the sample was in place and the excitation beam was directed onto the sample. Delayed PL spectra were measured by a 4Pi-cos gated-iCCD camera (Standford Computer Optics), excited by 360 nm pulsed laser generated from a fundamental Ti-sapphire laser (Coherent, Astrella, 5 mJ, 800 nm, 1 kHz). The thickness of the neat film was 200 nm.

DFT Calculation: All DFT calculations were done using the Gaussian 16 packages. The ω tuned ωB97X-D exchange-correlation functional was applied for all calculations.[45] The screening coefficient was tuned to equal the HOMO level and the calculated ionization energy, which coincides with Koopmans' theorem. The geometry optimizations for S_0 and S_1 were done using def2-SV(P) basis set. The basis sets were increased to def2-TZVP for the following single-point calculations. The implicit solvent of toluene was included in the formalism of the polarizable continuum model using the integral equation formalism variant (IEFPCM). Time-dependent density functional theory (TDDFT) was employed for the excited state calculations. The post-analysis was done using VMD and Multiwfn.[40,45–47]

XRD Measurement: The 1D X-ray diffraction patterns of thermally evaporated films were recorded in the 2θ manner between 3 and 50°, with a step of 0.01° and a speed of 10 degrees per min, using a Rigaku Smart Lab HR-XRD equipment in the ambient condition. The thickness of neat films was 50 nm.

Time-Correlated Single-Photon Counting (TCSPC): Time-resolved fluorescence intensity decay was measured using a picosecond laser at 375 nm. The decay in different time scales was measured by varying the laser pulse frequency. A rate of 1 MHz was used to monitor the prompt fluorescence and a 100 KHz laser was used to monitor the DF decay. Long-lived RTP decay was measured with the laser operating in the burst mode. The laser frequency was 1 MHz with 100 pulses for the excitation and then the following time the laser was off to monitor the RTP decay, with the total duty cycle time of 100 ms. The RTP decay fitting begins with a delay of 80 microseconds to exclude the impact of prompt and delayed fluorescence.

Fs-TA Spectroscopy Measurement: The fs-TA spectra were measured by using a Helios pump-probe setup (Ultrafast Systems), with an amplified 1030 nm laser (Pharos, Light Conversion, 200 fs, 200 μJ) with the repetition rate at 1 kHz. A small portion of the fundamental laser was directed to the optical delay stage, which was then used to generate broadband probe light by focusing on sapphire (visible range) or YAG (NIR range) crystals. The pump pulse at 360 nm was generated with an optical parametric amplifier (Orpheus-F, Light Conversion). The pump power was 50 or 100 μW indicated. Materials were dissolved in degassed chloroform or cyclohexane in a concentration of 0.05 mg mL^{-1} and measured in 2 mm path-length cuvettes. The dynamic fitting for the fs-TA data was done by the surface Xplorer software from Ultrafast Systems.

Sample Preparation for Microscopy Imaging: The films were prepared by directly dropping the organic material in a solvent onto cleaned glass substrates and used with dried film after solvent evaporation. The films and crystals for time-resolved microscopy were prepared with oxygen plasma-treated gridded glass coverslip (ibid Grid-50) and sealed in a nitrogen glove box.

Time-Resolved Microscopy: The time-resolved phosphorescence images were performed based on the Thunder system (Leica) with a sCMOS camera (Leica DFC9000). A 390 nm LED was selected for the illumination, equipped with a quadband filter cube (the excitation filter 375–407, 462–496, 542–566, and 622–654 nm; the dichroic beam splitter 415, 500, 572, 660 nm and the emission filter 420–450, 506–532, 578–610, and 666–724 nm). The same LED and corresponding quadband filter cube were selected for the fluorescence and phosphorescence channels, except that the LED for the phosphorescence channel was off. The phosphorescence images were acquired with a camera exposure time of 500 ms and 6 s for each frame, separately. After the film/crystal was continuously excited by the LED, after 19 ms, the phosphorescence images were recorded with an 11 ms interval between each phosphorescence image. For each sample, the brightness/intensity range of all phosphorescence images was set to the same as that of the first phosphorescence image.

Supporting Information

Supporting Information is available from the Wiley Online Library or from the author.

Acknowledgements

D.D., X.Z., and T.W. contributed equally to this work. The authors appreciated Dr. Dieter Schollmeyer from the University of Mainz for his help with the single crystal X-ray diffraction measurements. The assisstant for the HPLC measurements from Ms. Beate Mueller from Max Planck Institute for Polymer Research was highly appreciated. Computational studies were supported by the US National Science Foundation (CHE-2154346 to X.L. and T.W.).

Open access funding enabled and organized by Projekt DEAL.

Conflict of Interest

The authors declare no conflict of interest.

Data Availability Statement

The data that support the findings of this study are available from the corresponding author upon reasonable request.

Keywords

amorphous film, intramolecular steric hindrance, organic luminescent materials, room-temperature phosphorescence, through-space charge-transfer

Received: June 24, 2024
Revised: August 16, 2024
Published online: September 17, 2024

[1] P. Xviii, C. M. Braams, *Physica* **1952**, *29*, 431.
[2] J. Zhao, W. Wu, J. Sun, S. Guo, *Chem. Soc. Rev.* **2013**, *42*, 5323.
[3] T. Theiss, S. Buss, I. Maisuls, R. López-Arteaga, D. Brünink, J. Kösters, A. Hepp, N. L. Doltsinis, E. A. Weiss, C. A. Strassert, *J. Am. Chem. Soc.* **2022**, *145*, 3937.
[4] L. Chen, D. J. Hayne, E. H. Doeven, J. Agugiaro, D. J. D. Wilson, L. C. Henderson, T. U. Connell, Y. H. Nai, R. Alexander, S. Carrara, C. F. Hogan, P. S. Donnelly, P. S. Francis, *Chem. Sci.* **2019**, *10*, 8654.
[5] H. Lu, X. Jiang, Y. Chen, K. Peng, Y. Huang, H. Zhao, Q. Chen, F. Lv, L. Liu, S. Wang, Y. Ma, *Nanoscale* **2020**, *12*, 14061.
[6] T. B. Gao, J. J. Zhang, R. Q. Yan, D. K. Cao, D. Jiang, D. Ye, *Inorg. Chem.* **2018**, *57*, 4310.
[7] R. Kabe, N. Notsuka, K. Yoshida, C. Adachi, *Adv. Mater.* **2016**, *28*, 655.
[8] O. Bolton, K. Lee, H. J. Kim, K. Y. Lin, J. Kim, *Nat. Chem.* **2011**, *3*, 205.
[9] J. Zhang, S. Xu, L. Zhang, X. Wang, Y. Bian, S. Tang, R. Zhang, Y. Tao, W. Huang, R. Chen, *Adv. Mater.* **2022**, *34*, 2110547.
[10] Z. An, C. Zheng, Y. Tao, R. Chen, H. Shi, T. Chen, Z. Wang, H. Li, R. Deng, X. Liu, W. Huang, *Nat. Mater.* **2015**, *14*, 685.
[11] Y. Xiong, Z. Zhao, W. Zhao, H. Ma, Q. Peng, Z. He, X. Zhang, Y. Chen, X. He, J. W. Y. Lam, B. Z. Tang, *Angew. Chem., Int. Ed.* **2018**, *57*, 7997.
[12] Y. Xie, Y. Ge, Q. Peng, C. Li, Q. Li, Z. Li, *Adv. Mater.* **2017**, *29*, 1606829.
[13] L. Gu, W. Ye, X. Liang, A. Lv, H. Ma, M. Singh, W. Jia, Z. Shen, Y. Guo, Y. Gao, H. Chen, D. Wang, Y. Wu, J. Liu, H. Wang, Y. X. Zheng, Z. An, W. Huang, Y. Zhao, *J. Am. Chem. Soc.* **2021**, *143*, 18527.
[14] J. Song, L. Ma, S. Sun, H. Tian, X. Ma, *Angew. Chem., Int. Ed.* **2022**, *61*, e202206157.
[15] S. Hirata, *Adv. Opt. Mater.* **2017**, *5*, 1700116.
[16] M. S. Kwon, D. Lee, S. Seo, J. Jung, J. Kim, *Angew. Chem., Int. Ed.* **2014**, *53*, 11177.
[17] C. Chen, Z. Chi, K. C. Chong, A. S. Batsanov, Z. Yang, Z. Mao, Z. Yang, B. Liu, *Nat. Mater.* **2021**, *20*, 175.
[18] H. Shu, L. Chen, X. Wu, T. Wang, S. Wang, H. Tong, L. Wang, *J. Mater. Chem. C* **2022**, *10*, 1833.
[19] A. J. Gillett, A. Privitera, R. Dilmurat, A. Karki, D. Qian, A. Pershin, G. Londi, W. K. Myers, J. Lee, J. Yuan, S. J. Ko, M. K. Riede, F. Gao, G. C. Bazan, A. Rao, T. Q. Nguyen, D. Beljonne, R. H. Friend, *Nature* **2021**, *597*, 666.
[20] T. F. Hinrichsen, C. C. S. Chan, C. Ma, D. Paleček, A. Gillett, S. Chen, X. Zou, G. Zhang, H. L. Yip, K. S. Wong, R. H. Friend, H. Yan, A. Rao, P. C. Y. Chow, *Nat. Commun.* **2020**, *11*, 5617.
[21] M. Zeng, W. Wang, S. Zhang, Z. Gao, Y. Yan, Y. Liu, Y. Qi, X. Yan, W. Zhao, X. Zhang, N. Guo, H. Li, H. Li, G. Xie, Y. Tao, R. Chen, W. Huang, *Nat. Commun.* **2024**, *15*, 3598.
[22] S. Hirata, K. Totani, J. Zhang, T. Yamashita, H. Kaji, S. R. Marder, T. Watanabe, C. Adachi, *Adv. Funct. Mater.* **2013**, *23*, 3386.

[23] J. Guo, C. Yang, Y. Zhao, *Acc. Chem. Res.* **2022**, *55*, 1160.
[24] Y. Su, S. Z. F. Phua, Y. Li, X. Zhou, D. Jana, G. Liu, W. Q. Lim, W. K. Ong, C. Yang, Y. Zhao, *Sci. Adv.* **2018**, *4*, eaas9732.
[25] W. Xu, Y. Yu, X. Ji, H. Zhao, J. Chen, Y. Fu, H. Cao, Q. He, J. Cheng, *Angew. Chem., Int. Ed.* **2019**, *58*, 16018.
[26] C. Wu, W. Liu, K. Li, G. Cheng, J. Xiong, T. Teng, C. M. Che, C. Yang, *Angew. Chem., Int. Ed.* **2021**, *60*, 3994.
[27] X. Lv, Y. Wang, N. Li, X. Cao, G. Xie, H. Huang, C. Zhong, L. Wang, C. Yang, *Chem. Eng. J.* **2020**, *402*, 126173.
[28] X. Tang, L. S. Cui, H. C. Li, A. J. Gillett, F. Auras, Y. K. Qu, C. Zhong, S. T. E. Jones, Z. Q. Jiang, R. H. Friend, L. S. Liao, *Nat. Mater.* **2020**, *19*, 1332.
[29] Y. Li, Q. Wei, L. Cao, F. Fries, M. Cucchi, Z. Wu, R. Scholz, S. Lenk, B. Voit, Z. Ge, S. Reineke, *Front. Chem.* **2019**, *7*, 688.
[30] C. Jiang, J. Miao, D. Zhang, Z. Wen, C. Yang, K. Li, *Research* **2022**, 9892802.
[31] J. Yu, H. Ma, W. Huang, Z. Liang, K. Zhou, A. Lv, X. G. Li, Z. He, *JACS Au* **2021**, *1*, 1694.
[32] S. Shao, J. Hu, X. Wang, L. Wang, X. Jing, F. Wang, *J. Am. Chem. Soc.* **2017**, *139*, 17739.
[33] Y. Mu, Z. Yang, J. Chen, Z. Yang, W. Li, X. Tan, Z. Mao, T. Yu, J. Zhao, S. Zheng, S. Liu, Y. Zhang, Z. Chi, J. Xu, M. P. Aldred, *Chem. Sci.* **2018**, *9*, 3782.
[34] L. S. Cui, A. J. Gillett, S. F. Zhang, H. Ye, Y. Liu, X. K. Chen, Z. Sen Lin, E. W. Evans, W. K. Myers, T. K. Ronson, H. Nakanotani, S. Reineke, J. L. Bredas, C. Adachi, R. H. Friend, *Nat. Photonics* **2020**, *14*, 636.
[35] S. Kuno, H. Akeno, H. Ohtani, H. Yuasa, *Phys. Chem. Chem. Phys.* **2015**, *17*, 15989.
[36] J. Yang, X. Zhen, B. Wang, X. Gao, Z. Ren, J. Wang, Y. Xie, J. Li, Q. Peng, K. Pu, Z. Li, *Nat. Commun.* **2018**, *9*, 840.
[37] D. K. A. Phan Huu, S. Saseendran, R. Dhali, L. G. Franca, K. Stavrou, A. Monkman, A. Painelli, *J. Am. Chem. Soc.* **2022**, *144*, 15211.
[38] S. Y. Yang, Y. K. Wang, C. C. Peng, Z. G. Wu, S. Yuan, Y. J. Yu, H. Li, T. T. Wang, H. C. Li, Y. X. Zheng, Z. Q. Jiang, L. S. Liao, *J. Am. Chem. Soc.* **2020**, *142*, 17756.
[39] Z. Yin, M. Gu, H. Ma, X. Jiang, J. Zhi, Y. Wang, H. Yang, W. Zhu, Z. An, *Angew. Chem., Int. Ed.* **2021**, *60*, 2058.
[40] E. A. Margulies, C. E. Miller, Y. Wu, L. Ma, G. C. Schatz, R. M. Young, M. R. Wasielewski, *Nat. Chem.* **2016**, *8*, 1120.
[41] X. Ma, C. Xu, J. Wang, H. Tian, *Angew. Chem.* **2018**, *130*, 11020.
[42] D. Li, F. Lu, J. Wang, W. Hu, X. M. Cao, X. Ma, H. Tian, *J. Am. Chem. Soc.* **2018**, *140*, 1916.
[43] X. Peng, P. Zou, J. Zeng, X. Wu, D. Xie, Y. Fu, D. Yang, D. Ma, B. Z. Tang, Z. Zhao, *Angew. Chem., Int. Ed.* **2024**. 202405418.
[44] J. Mello, H. Wittmann, R. Friend, *Adv. Mater.* **1997**, *9*, 230.
[45] J. D. Chai, M. Head-Gordon, *Phys. Chem. Chem. Phys.* **2008**, *10*, 6615.
[46] T. Lu, F. Chen, *J. Comput. Chem.* **2012**, *33*, 580.
[47] G. Tocci, L. Joly, A. Michaelides, *Nano Lett.* **2014**, *14*, 6872.